Journal of
Marine Science and Engineering

MDPI

Article

A Novel Acoustic Method for Cavitation Identification of Propeller

Yang Li and Lilin Cui *

National Key Laboratory on Ship Vibration and Noise, Naval University of Engineering, Wuhan 430033, China
* Correspondence: cuililinwyt@163.com

Abstract: When a propeller is under a state of cavitation, it will experience negative effects, including strong noise, vibration, and even damage to the blades. Accordingly, the detection of propeller cavitation has attracted the attention of researchers. Propeller noise signal contains a wealth of cavitation information, which is a powerful method to identify the cavitation state. Considering the nonlinear characteristics of propeller noise, a feature describing the complexity of nonlinear signals, which is called refined composite multiscale fluctuation-based dispersion entropy (RCMFDE), is adopted as the indicator of propeller cavitation, and a framework for the identification of propeller cavitation state is established in this paper. Firstly, the propeller noise signal is decomposed by the complete ensemble empirical mode decomposition with adaptive noise (CEEMDAN) method, and the intrinsic mode function (IMF) components with cavitation characteristics are extracted. Secondly, the RCMFDE of the IMF components is computed. Finally, a hybrid optimization support vector machine (SVM) is established to classify the features, in which a Relief-F filter is utilized to reduce the feature dimension, and a particle swarm optimization (PSO) wrapper is utilized to optimize the parameters of the SVM. The experimental results demonstrate encouraging accuracy to apply this approach to identify the propeller cavitation states, with an identification accuracy of 91.11%.

Keywords: RCMFDE; cavitation noise; feature extraction; machine learning

Citation: Li, Y.; Cui, L. A Novel Acoustic Method for Cavitation Identification of Propeller. *J. Mar. Sci. Eng.* **2022**, *10*, 1225. https://doi.org/10.3390/jmse10091225

Academic Editor: Alon Gany

Received: 24 July 2022
Accepted: 29 August 2022
Published: 1 September 2022

1. Introduction

Cavitation is a general fluid mechanics phenomenon that can occur in the operation of a marine propeller [1]. The speed at which cavitation starts is called the cavitation inception speed (CIS) when the vessel is drifting steadily. When the propeller speed is higher than CIS or in some off-design conditions, the pressure in the low-pressure area at the tip and back surface of propeller blade is lower than the saturated vapor pressure, and cavitation forms [2]. Propeller cavitation can produce many undesirable consequences. On the one hand, the jet flow produced by a cavitation bubble bursting acts on the propeller blade for a long time, leading to cavitation erosion phenomenon, causing damage to the blades [3]. On the other hand, cavitation will induce strong noise and vibration, which becomes the main noise source of vessels, affecting the acoustic stealth of vessels and the comfort of the crew's living environment, and negatively affecting marine mammals and the ecological environment [4]. As a complex nonlinear phenomenon, there are many factors affecting the cavitation process [5], and accurate prediction of the cavitation of a full-scale propeller cannot be achieved at present, so that only the real-time monitoring method can be used to obtain the cavitation state of a propeller during navigation. Early detection of propeller cavitation helps the operator to adjust the working conditions of the propeller in time and avoid the negative effects caused by cavitation. Consequently, an accurate cavitation detection method of propellers is of critical importance.

The optics-based approach is a direct way to detect cavitation. When cavitation occurs, traveling or banded bubbles appear near the mechanical blade, which can be directly observed by the naked eye or with the help of stroboscopic equipment, high-speed camera

and other optical devices [3]. However, in practical engineering, the application of the optical method is confined by factors such as fluid visibility and ambient brightness, so indirect detection methods based on vibration, sound and pressure fluctuation have been proposed and applied in the past few years. Generally speaking, these detection methods comprise three steps: signal preprocessing, feature extraction and classification.

As for the signal preprocessing method, because of the non-stationarity of cavitation noise, some non-stationary signal analysis methods, such as short-time Fourier transform (STFT) [6], wavelet scalogram [7], wavelet packet [8], Wigner-Ville distribution (WVD) [9], time-domain synchronous averaging (TSA) [10] and empirical mode decomposition (EMD) [11], have been applied to the analysis of cavitation signals. Nevertheless, these methods have some shortcomings: STFT and wavelet methods are limited by basis functions and do not have adaptability; WVD has the problem of cross-term aliasing. TSA involves a complex resampling procedure; although EMD is an adaptive method, the modal aliasing problem limits its application. CEEMDAN is an improved algorithm based on EMD, which adaptively adds white noise to each layer decomposition process to better suppress mode aliasing, reduce residual noise and improve the integrity and efficiency of decomposition [12]. Due to these advantages, CEEMDAN has been applied to non-stationary signal processing in fields such as fault diagnosis [13], biological signal processing [14], and power prediction [15], however, to our best knowledge, its application in cavitation noise signal processing has not been reported.

As for feature extraction, traditional cavitation detection methods are typically based on the energy [16,17] and modulation characteristics [18,19] of the signal. Since the formation, development and collapse of cavitation bubbles is a nonlinear process, and only using energy or demodulation characteristics to describe cavitation characteristics is incomplete. As a nonlinear analysis technique, entropy has been widely used in feature extraction in recent years [20–22]. Fluctuation-based dispersion entropy (FDE) is a kind of nonlinear dynamical entropy. Compared with permutation entropy, sample entropy and fuzzy entropy, FDE enjoys a better performance in terms of stability, calculation cost and noise-robustness [23]. However, FDE can only evaluate the dynamic characteristics of time series on a single scale, which leads to serious information loss. In order to obtain deeper signal features from different scales, multi-scale [24], composite multi-scale [25] and fine composite multi-scale [26] methods are proposed. Compared with the previous two methods, the fine composite multi-scale has better stability and performance effect. Up to now, there are few studies on entropy in the field of cavitation feature extraction. Considering the advantages of FDE and the requirements of multi-scale analysis, this paper combines the fine composite multi-scale method and FDE to form RCMFDE, which is used to represent the characteristics of propeller cavitation state.

After feature extraction, it is essential to choose an appropriate classification algorithm to intelligently identify the feature. Common machine learning classification algorithms include back propagation neural networks (BPNN), random forest (RF) and SVM. BPNN is sensitive to the initial weight of the network, and when the network is initialized with different weights, the BP algorithm can run into the local minimum problems. Random forest is susceptible to overfitting problems when dealing with classification problems affected by noise. SVM is a supervised machine learning classification model which can effectively deal with local minimum and overfitting problems in BPNN and RF, and has been successfully applied to the classification of features such as multiscale entropy in the fault diagnosis field [27,28]. However, the multi-scale entropy feature usually has a high dimension, which affects the training efficiency, and the setting of SVM model parameters also has a great influence on the classification effect. Thus, it is essential to take measures to optimize the classification model.

In this paper, a novel acoustic method for intelligent identification of propeller cavitation state based on CEEMDAN, RCMFDE, and hybrid optimization SVM is proposed. Firstly, CEEMDAN is applied to preprocess propeller noise to adaptively separate cavitation characteristic signals from propeller noise signals and reduce the influence of mode

aliasing. Then, the RCMFDE algorithm is applied to extract the nonlinear complexity features of noise signals at different scales and the cavitation state of propeller can be distinguished from the perspective of nonlinear characteristics. Finally, to solve the problem of feature redundancy and parameter optimization, a hybrid optimization SVM classification model is established to realize intelligent identification of propeller cavitation and a higher identification accuracy is achieved. The rest of this paper is organized as follows. Section 2 introduces the basic principles and framework of the proposed method. Section 3 introduces the cavitation noise measurement experiment of the propeller model. In Section 4, the experimental data are analyzed based on the method proposed in this paper and compared with other methods. Finally, Section 5 is the conclusion of this paper.

2. Identification for Cavitation States of Propeller Based on CEEMDAN-RCMFDE and Hybrid Optimization SVM

2.1. CEEMDAN Principle

CEEMDAN is an improved algorithm based on EMD, which references the idea of adding gaussian noise and removing noise through multiple averaging in EEMD method [12,13]. To better illustrate the principle, $E_k(\cdot)$ is defined as the k-th IMF component obtained after EMD, and $v_i(t)$ represents the white noise component with N (0,1) added in the i-th test. For signal $X(t)$, the steps of CEEMDAN method are as follows:

(1) Construct the signal that adds noise $X_i(t) = X(t) + \varepsilon_0 v_i(t)$, where ($i$ = 1, 2, . . . , I), ε_0 is the amplitude, and I is the number of the experiment. Decompose by EMD I realization $X_i(t)$ to get first IMF and calculate:

$$IMF_1(t) = \frac{1}{I}\sum_{i=1}^{I} E_1(X_i(t)) \tag{1}$$

(2) At the first stage (k = 1), the first residual is calculated as:

$$r_1(t) = X(t) - IMF_1(t) \tag{2}$$

(3) Decompose realizations $r_1(t) + \varepsilon_1 E_1(v_i(t)), i = 1, 2, \ldots, I$. Get their first EMD mode and define the second mode:

$$IMF_2(t) = \frac{1}{I}\sum_{i=1}^{I} E_1(r_1(t) + \varepsilon_1 E_1(v_i(t))) \tag{3}$$

(4) The calculation of the latter mode is consistent with step 3. First, the k-th residual signal is calculated, and then the (k + 1)-th mode is calculated, as shown in Equations (4) and (5):

$$r_k(t) = r_{k-1}(t) - IMF_k(t) \tag{4}$$

$$IMF_{k+1}(t) = \frac{1}{I}\sum_{i=1}^{I} E_1(r_k(t) + \varepsilon_k E_k(v_i(t))) \tag{5}$$

(5) Decomposition stops until the residual is a monotone function. The final residual is as shown in

$$R(t) = X(t) - \sum_{k=1}^{K} IMF_k(t) \tag{6}$$

Then, the original signal $X(t)$ is expressed as shown in Equation (7):

$$X(t) = \sum_{k=1}^{K} IMF_k(t) + R(t) \tag{7}$$

2.2. RCMFDE Algorithm

2.2.1. FDE

Fluctuation-based dispersion entropy (FDE) is an index to measure the irregularity of a time series, which takes into account the local fluctuation characteristics of series and can effectively express the nonlinear characteristics of the signal [29]. For a given nonlinear time series $x = \{x_1, x_2, \ldots x_N\}$, the calculation procedure of FDE is as follows:

(1) Establish the mapping between time series x and $\{1, 2, \ldots, c\}$ using the Equation (8)

$$y_i = \frac{1}{\sigma\sqrt{2\pi}} \int_{-\infty}^{x_i} e^{-\left(-\frac{(t-\mu)^2}{2\sigma^2}\right)} dt \tag{8}$$

$$z_j^c = round(c \cdot y_i + 0.5) \tag{9}$$

where μ is expectation and σ^2 is variance, and c is an integer.

(2) Calculate the embedded vector Z as follows:

$$Z_j^{m,\lambda,c} = \left\{ z_j, z_{j+\lambda}, \ldots, z_{j+(m-1)\lambda} \right\} \tag{10}$$

where m is the embedding dimension, λ is the time delay, and $j = 1, 2, \ldots, N - (m-1)\lambda$.

(3) Transform $Z^{m,\lambda,c}$ to $Q^{m,\lambda,c}$ by

$$Q_j^{m,\lambda,c} = \left\{ z_{j+\lambda} - z_j, \ldots, z_{j+(m-1)\lambda} - z_{j+(m-2)\lambda} \right\} \tag{11}$$

(4) For each time series $Q^{m,\lambda,c}$, there is a corresponding fluctuation dispersion pattern $\Pi_{v_0 v_1 \ldots v_{m-2}} (1 - c \le v \le c - 1)$, where $Q_{j,1}^{m,\lambda,c} = v_0, Q_{j,2}^{m,\lambda,c} = v_1, \ldots, Q_{j,m-1}^{m,\lambda,c} = v_{m-2}$. The relative frequency of each pattern is calculated by:

$$p\left(\Pi_{v_0 v_1 \ldots v_{m-2}}\right) = \frac{Number\left(\Pi_{v_0 v_1 \ldots v_{m-2}}\right)}{N - (m-1)\lambda} \tag{12}$$

where $Number\left(\Pi_{v_0 v_1 \ldots v_{m-2}}\right)$ represents the number of $Q^{m,\lambda,c}$ mapped to $\Pi_{v_0 v_1 \ldots v_{m-2}}$.

(5) According to the definition of Shannon entropy, the FDE of original time series x is defined as

$$FDE(X, m, c, \lambda) = -\sum_{\pi=1}^{(2c-1)^{m-1}} p\left(\Pi_{v_0 v_1 \ldots v_{m-2}}\right) ln\ p\left(\Pi_{v_0 v_1 \ldots v_{m-2}}\right) \tag{13}$$

2.2.2. RCMFDE

FDE is the characteristic of signal sequence at a single scale. Combined with refined composite multiscale analysis, refined composite multiscale fluctuation-based dispersion entropy (RCMFDE) can reflect the complexity relationship of signals at different scales [22]. The calculation procedure of RCMFDE for $x = \{x_1, x_2, \ldots x_N\}$ is as follows:

(1) The n-th coarse-grained time series $e_n = \left(e_{n,1}, e_{n,2}, \ldots, e_{n,(N/\tau)}\right)$ is obtained by Equation (14):

$$e_{n,k} = \frac{1}{\tau} \sum_{i=n+\tau(k-1)}^{n+k\tau-1} x_i \tag{14}$$

where τ is the scale factor, $1 < n < \tau, 1 < k < N/\tau$.

(2) RCMFDE is calculated by

$$RCMFDE(X, m, c, \lambda, \tau) = -\sum_{\pi=1}^{(2c-1)^{m-1}} \overline{p}\left(\Pi_{v_0 v_1 \ldots v_{m-2}}\right) \ln\ \overline{p}\left(\Pi_{v_0 v_1 \ldots v_{m-2}}\right) \tag{15}$$

where $\overline{p}\left(\Pi_{v_0 v_1 \ldots v_{m-2}}\right)$ is the mean frequency of the same dispersion patterns in each coarse-grained time series.

The parameters involved are delay λ, embedding dimension m, class number c and scale factor τ. If the embedding dimension m is too small, the dynamic changes might not be detected in the signal, while a large m may make the FDE algorithm unable to observe small variations [30]. For the number of classes c, its value should be greater than 1 to avoid that there is only a dispersed pattern. At the same time, a small c value leads to poor resolution, but a huge c value is easy to introduce noise effects, and the scope of c is commonly 4 to 8. For delay λ, the value is normally 1 to avoid loss of frequency information. For the scale factor τ, if the value is too small, the characteristic information of the series will be insufficient, but if the value is too large, the amount of calculation will be increased. Regarding the calculation accuracy and efficiency, the embedding dimension m = 3, the number of classes c = 6 and the scale factor τ = 20 is adopted in this paper.

2.3. Hybrid Optimization SVM Classification Model

When applied in the classification of features similar to multiscale entropy, there are two problems with SVM classification model as follows: first, the feature dimension is high and there is a certain redundancy, which leads to low computational efficiency. The other is that when kernel function is introduced to deal with nonlinear problems, the penalty factor c and the kernel parameter g have a great influence on the final classification effect, and it is considered unreliable to determine the two parameters only by experience. To solve these two problems, a hybrid optimization SVM based on Relief-F and PSO is proposed in this paper.

2.3.1. Relief-F

Relief-F method is an efficient filter-based feature selection method, which can rank the features by analyzing the relevant weight between features and classifications [31]. Assume that the samples in dataset D come from γ categories. For feature x_i, if it belongs to class $k \in \{1, 2, \ldots \gamma\}$, firstly the method looks for the nearest neighbor example of x_i in the k-th class sample $x_{i,nh}$ as near-hit, and then finds a nearest neighbor example of x_i in each class outside the k-th class as near-miss, denoted by $x_{i,l,nm}(l = 1, 2, \ldots \gamma; l \neq k)$. Thus, the relevance level corresponding to feature j is:

$$\delta^j = \sum_i -diff\left(x_i^j, x_{i,nh}^j\right)^2 + \sum_{l \neq k}\left(p_l \times diff\left(x_i^j, x_{i,l,nm}^j\right)^2\right) \tag{16}$$

where p_l is the proportion of class L samples in data set D. For each feature, the larger the relevance level, the better the classification ability of the corresponding attribute is.

2.3.2. PSO Algorithm

PSO is a classical swarm intelligent algorithm designed by simulating the predation behavior of birds, which has the advantages of good robustness, good convergence and strong global search ability. When applied to SVM model parameter optimization, it can effectively solve the problem of blind parameter setting [13]. In the algorithm, the global optimal solution is achieved by iteratively updating the position of particle swarm according to Equations (17) and (18) [32].

$$v_{id}^k = wv_{id}^{k-1} + c_1 r_1\left(pbset_{id} - x_{id}^{k-1}\right) + c_2 r_2\left(gbset_{id} - x_{id}^{k-1}\right) \tag{17}$$

$$x_{id}^k = x_{id}^{k-1} + v_{id}^{k-1} \tag{18}$$

where v_{id}^k is the motion velocity of the k-th iteration particle, x_{id}^k is the position of the k-th iteration particle in the current search space, c_1 and c_2 are acceleration factors, r_1 and r_2 are two random constants in the value range, w is the inertial weight, $pbset_{id}$ is the historical

optimal position of a single particle and $gbset_{id}$ is the historical optimal position of the particle swarm.

2.3.3. Hybrid Optimization SVM Based on Relief-F and PSO

The flow chart of the hybrid optimization SVM based on Relief-F and PSO is shown in Figure 1. In the model, Relief-F filter is utilized to reduce the feature dimension, improving the calculation efficiency and PSO wrapper to optimized parameter combination (c, g) for better accuracy. The specific steps are as follows:

(1) Use the Relief-F method to rank the features of the training sets from the highest best feature to the lowest using Equation (16).
(2) Initialize parameters, including particle number, learning factor, weighting coefficient, particle position and particle velocity, and the penalty factor c and kernel parameter g of SVM are encoded as the position of the particle.
(3) Train SVM model with the training set. The parameters c and g vary as the particle travels.
(4) Assess the fitness values. The SVM corresponding to each particle is used to predict the training sample, and the prediction error of the current particle is taken as the fitness of the particle.
(5) Determine whether the termination condition is satisfied. If the set ideal accuracy rate or number of iterations is attained, the iteration is discontinued. Otherwise, update the velocity and position of the particle swarm and resume step 3 to 5.
(6) Load optimal parameters acquired to model and classify the test set.

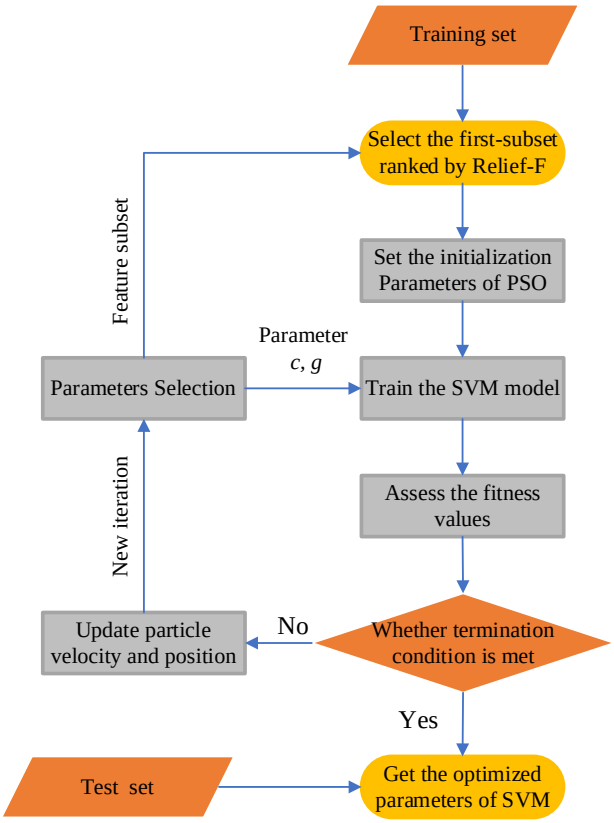

Figure 1. Algorithm flow of the hybrid optimization SVM based on Relief-F and PSO.

2.4. Steps of Cavitation State Identification for Propeller Noise Signal

In this paper, an intelligent propeller cavitation state identification method integrated CEEMDAN, RCMFDE, hybrid optimization SVM is proposed and its flow chart is shown in Figure 2. The specific implementation steps include:

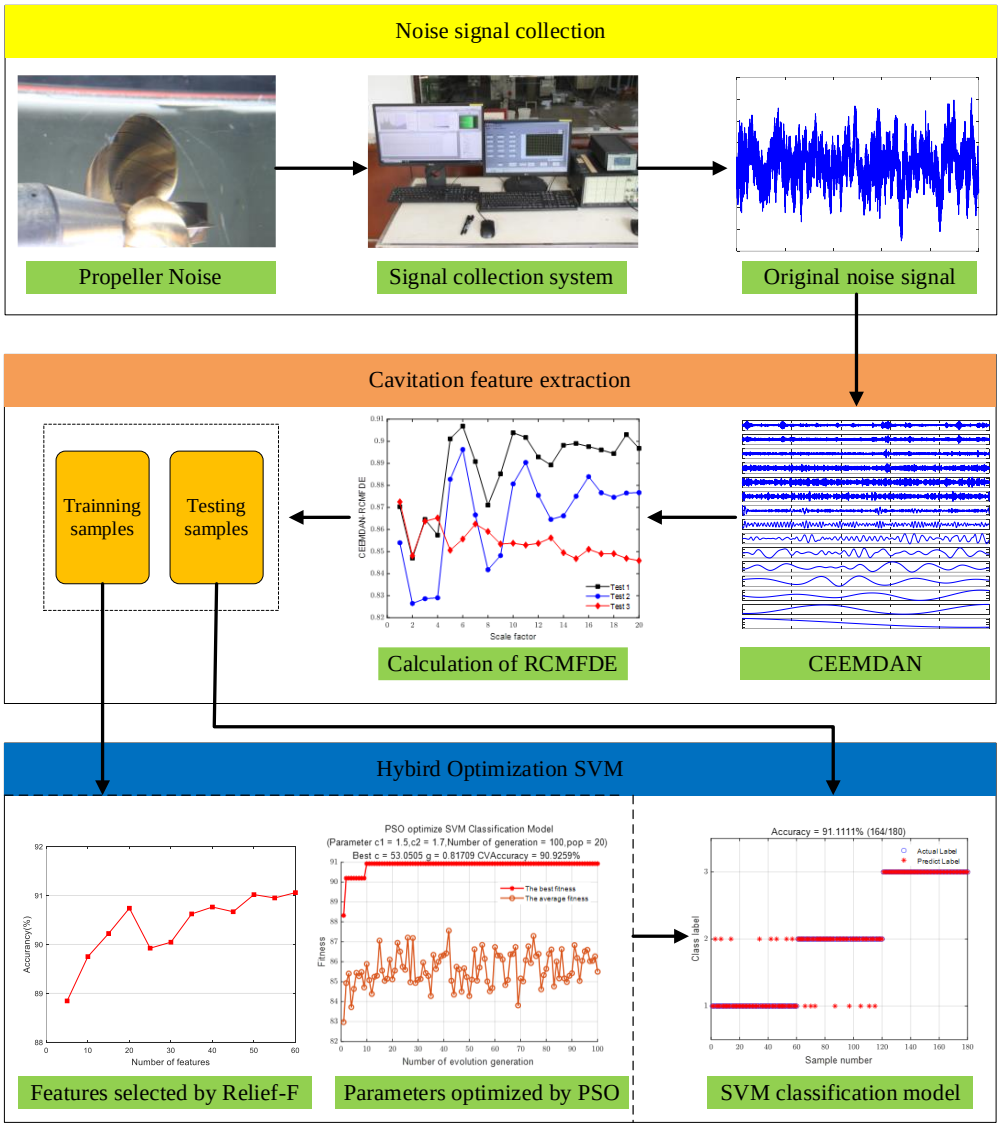

Figure 2. Flow chart of propeller cavitation state identification based on the proposed method.

Step 1. Carry out propeller model noise measurement test in cavitation tunnel, and collect propeller noise signals under different cavitation states.

Step 2. CEEMDAN is applied to decompose the origin signal into several modal components. IMF components associated with cavitation were extracted.

Step 3. Calculate the RCMFDE value of the extracted IMF component at 20 scales to form the signal feature vector.

Step 4. The hybrid optimization SVM model is trained by the training set and the optimized parameters, including features subset, penalty factor c and kernel parameter g are acquired. Then the test sample set is used to test the model.

3. Experimental Investigation

The acoustic measurement experiment of propeller model was carried out in the medium-sized cavitation tunnel of China Ocean Shipping Company (COSCO). The schematic diagram of the cavitation tunnel is shown in Figure 3. There is a four-blade axial pump at the bottom of the cavitation tunnel, which is driven by a DC shunt motor. By adjusting the power of the motor, the flow velocity of water in the tunnel can be precisely regulated. The tunnel is equipped with a pressure regulating device that can fine-tune the internal pressure within a certain range.

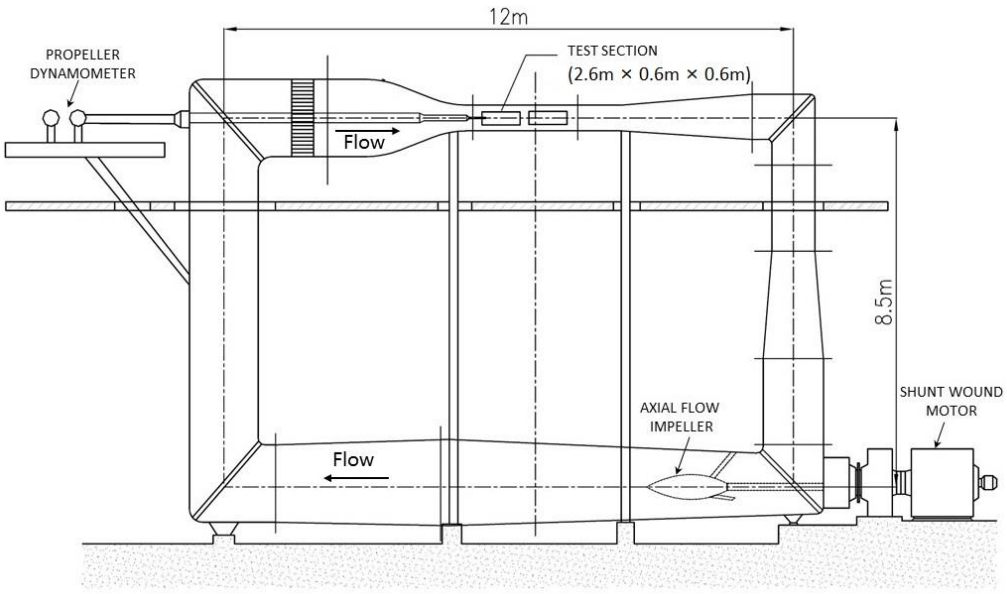

Figure 3. General arrangement of the cavitation tunnel.

The test section is the core part of the cavitation tunnel, where the propeller is located and works in the given stable flow field. The test section lies in the upper middle part of the device, as shown in Figure 4. The length of the test section is 2.6 m, and the cross section is rectangular (0.6 m × 0.6 m) with rounded corners. The four sides of the test section are view windows made by acoustically transparent acrylic, through which the cavitation of the propeller can be observed from all around with the help of stroboscopic equipment. The propeller dynamometer drives the propeller in the test section through a long shaft and measures its thrust, torque and rotation speed in real time. The basic parameters of the cavitation tunnel are summarized in Table 1.

Figure 4. The test section of the cavitation tunnel.

Table 1. Principal particulars of the cavitation tunnel.

Item	Value
Dimension of test section, length × width × height	2.6 m × 0.6 m × 0.6 m
Pressure range	10~200 kPa
Maximum velocity	12 m/s
Velocity instability	≤1%
Velocity unevenness	≤1%
Minimum cavitation number	0.2
Motor capacity	90 kW

A standard DTM4381 propeller model with a diameter of 180 mm is used in the experiment, and the basic information of the propeller is given in Table 2. The wake prosthesis contains a V-shaped bracket and a double hole wake grid is arranged in front of the propeller, which forms a non-uniform flow field close to the real ship. An acoustic tank full of water is suspended on the side of the test section, the size of which is 800 mm × 400 mm × 300 mm. One side of the tank is attached to the test section through the perspective window. A hydrophone (model: B&K 8104) is suspended freely in the tank. The hydrophone is in the same plane with the propeller disk, and is 500 mm away from the center of the propeller hub. The top view schematic diagram of the test section is shown in Figure 5 and the layout of the propeller model, wake prosthesis and hydrophone are shown in Figure 6. The propeller noise signal collected by hydrophone is amplified by charge amplifier (model: B&K 2690A), and then converted into digital signal by signal acquisition instrument (model: B&K LAN-XI 3161) and recorded. The parameters of the signal collection system are outlined in Table 3.

Table 2. Basic information of test propeller.

Parameter	Value
Number of blades	5
Diameter	180 mm
Pitch ratio	1.2
Area ratio	0.725
Boss ratio	0.2
Material	brass

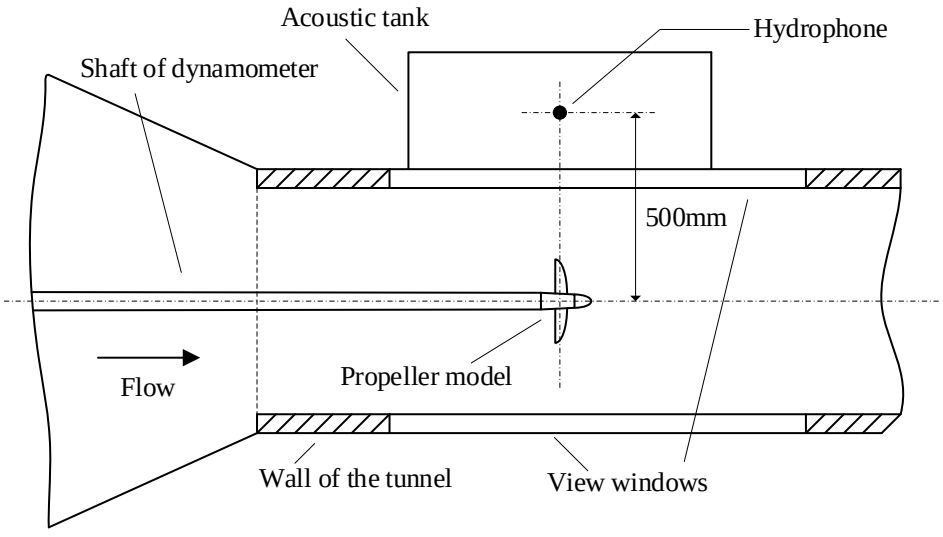

Figure 5. The top view schematic diagram of the test section.

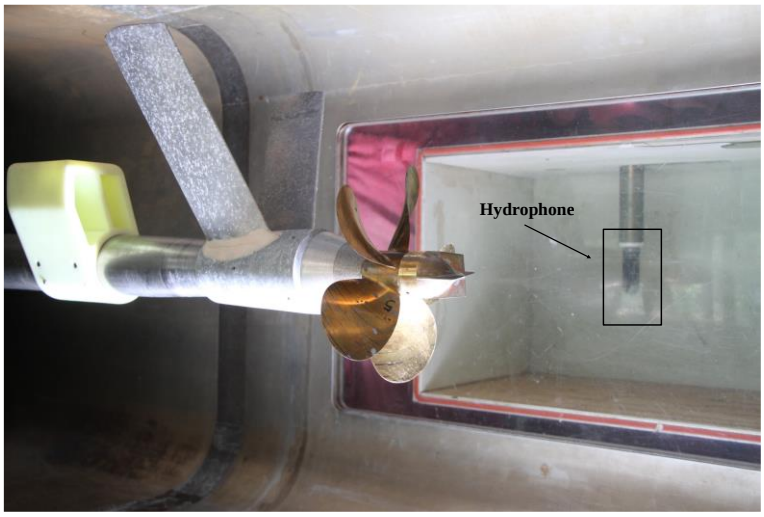

Figure 6. Layout of the propeller model, wake prosthesis and hydrophone.

Table 3. Parameters of the signal collection system.

Item	Model	Parameter
Hydrophone	B&K 8104	Frequency range: 0.1 Hz–120 kHz Charge sensitivity: 0.44 pC/Pa
Charge-amplifier	B&K 2690A	Frequency range: 0–100 kHz
Data Acquisition System	B&K LAN-XI 3161	Frequency range: 0–204.8 kHz

The propeller is tested at a prescribed set of two non-dimensional numbers [18]: thrust coefficient k_t and cavitation number σ_n:

$$k_t = \frac{T}{\rho n^2 D^4} = f\left(\frac{V}{nD}\right) \tag{19}$$

$$\sigma_n = \frac{p_0 - p_v}{\frac{1}{2}\rho n^2 D^2} \tag{20}$$

where T is the thrust force of propeller, ρ is the water density, n is the rotation speed of propeller, D is the diameter of propeller, V is the inflow velocity, $f(\cdot)$ is the mapping relationship of this propeller, p_0 is the pressure in the tunnel, and finally p_v is the saturated vapor pressure depending on temperature. In cavitation tunnel, k_t is adjusted by changing the ratio of inflow velocity V to rotational speed n, and σ_n is adjusted by changing the pressure p_0, and propeller rotation speed n. For propeller tip vortex cavitation (TVC), which most commonly occurs in the propeller of full-scale ships, when k_t (σ_n) remains constant, cavitation may occur or be serious with the decrease in σ_n (increase in k_t).

In our case, considering the efficiency of operation, the pressure p_0 and propeller rotation speed n are set as constant values to keep the cavitation number σ_n constant, and the thrust coefficient k_t is regulated by changing the pump power, so that the propeller appears different cavitation states. Through early testing, the initial pressure of the test, the propeller rotation speed and inflow velocity are determined, in which propeller cavitation does not occur. Then slowly decrease the flow velocity, and observe the propeller vortex cavitation at the same time with the help of a stroboscopic device. It is observed that there is no cavitation until the k_t exceeds 0.33, as the development of cavitation of propeller blades is not synchronous due to slight geometrical differences between blades. In this experiment, if only one blade exhibits cavitation it is regarded as cavitation inception, and 3 blades (more than half of whole 5 blades) exhibiting cavitation is full cavitation. The test

conditions of three cavitation states including no cavitation, cavitation inception and full cavitation is outlined in Table 4, and the images of propeller cavitation at three states are shown in Figure 7. The sampling frequency of noise signal is 131.072 kHz, and propeller noise data of 30 s are collected for each cavitation state.

Table 4. Test condition and cavitation state of the propeller model.

Test Number	Pressure p_0/kPa	Rotation Speed n/rps	Cavitation Number σ_n	Inflow Velocity V/m/s	Thrust Coefficient k_t	Cavitation State
1	103.2	28	7.93	4.69	0.24	No cavitation
2				3.54	0.33	Cavitation inception
3				3.32	0.35	Full cavitation

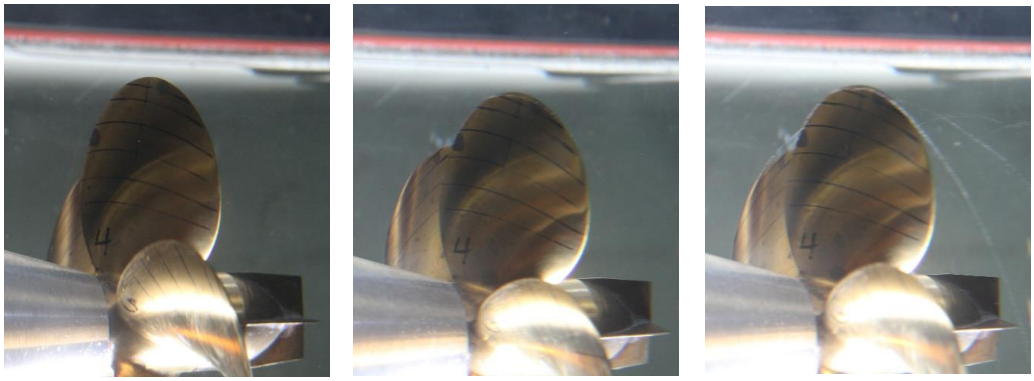

(**a**) (**b**) (**c**)

Figure 7. Images of propeller cavitation at three states: (**a**) no cavitation; (**b**) cavitation inception; (**c**) full cavitation.

4. Result and Discussion

4.1. Cavitation Feature Extraction by CEEMDAN-RCMRDE

The original time domain diagram of the propeller noise signal collected in the test under three test conditions is shown in Figure 8. It can be seen that the time domain waveform and amplitude of noise in the inceptive stage of propeller cavitation are close to that without cavitation. In the stage of full cavitation, the noise amplitude increases and the propeller beat becomes obvious. The power spectrum of noise calculated under three conditions is shown in Figure 9. It is apparent that the power spectral densities of test 1 and test 2 are close in the whole frequency range, only except the frequencies above 30 kHz. However, the power spectral density of test 3 is clearly higher than the other two tests at frequencies above 2.5 kHz. The energy increased by the full cavitation spans a quite wide frequency range.

Waveform and spectrum only reflect unilateral information of signal in time domain or frequency domain, respectively, while CEEMDAN, as an adaptive decomposition method, can decompose the signal into multiple IMF components, which can reflect the characteristics of signal in time domain and frequency domain at the same time. The raw noise signals under three test conditions are decomposed by the CEEMDAN method, in which the noise standard deviation of CEEMDAN is 0.2, the average number of signal processing is 50, and the maximum number of iterations is 100.

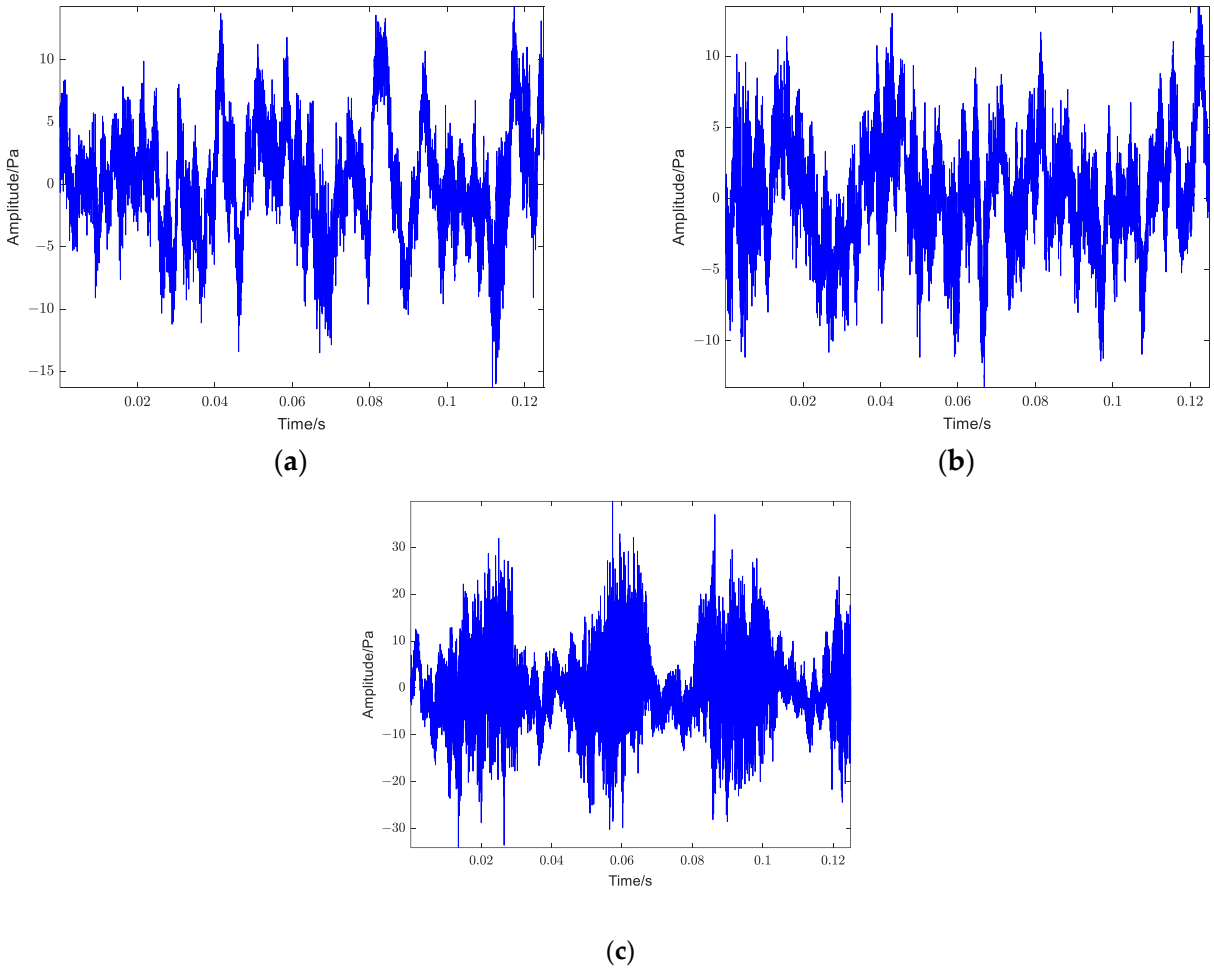

Figure 8. Original time domain diagram of propeller noise signal collected under three test conditions: (**a**) no cavitation; (**b**) cavitation inception; (**c**) full cavitation.

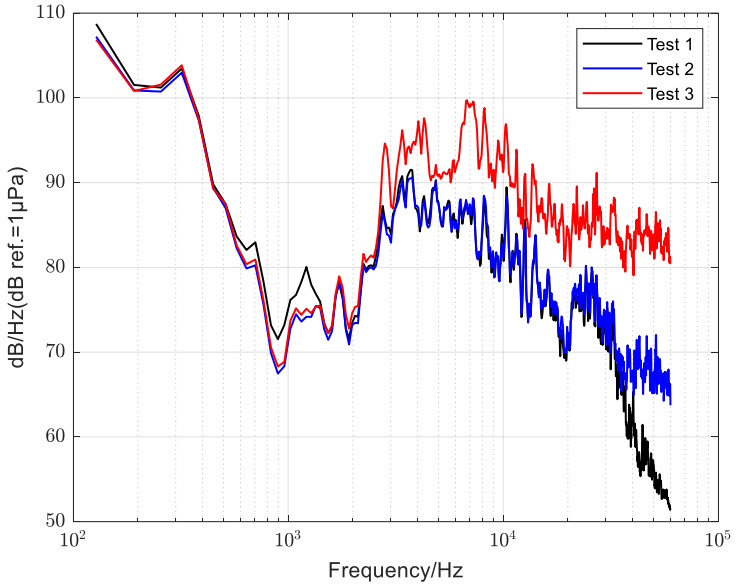

Figure 9. Power spectral densities for noise measurement; processing parameters: Hanning window, 50% overlapping, frequency resolution of 64 Hz.

Figure 10 shows the CEEMDAN results under three working conditions. In the figure, the time domain waveform of IMF component is illustrated on the left, and the corresponding power spectrum of IMF component is given on the right. With the increase in IMF orders, the spectral centroid moves from high frequency to low frequency. Since the low frequencies of the higher order components are usually independent with cavitation, only the first eight order components are listed in the figure. It can be seen that in Figure 10a, when cavitation does not occur, there is no obvious pulse signal in the low-order IMF components. While in Figure 10b, after cavitation occurs, pulses with the same rotation period of the propeller (about 35 ms) appear in IMF1 and IMF2, and in Figure 10c, distinct periodic pulses propagate from IMF1 and IMF2 to low frequency band and appear in IMF3 to IMF6, which is consistent with the results of power spectral analysis. According to the frequency band range of cavitation energy influence in power spectrum analysis and the frequency band range of IMF signal, the first three IMF components are selected as cavitation characteristic signals in the test.

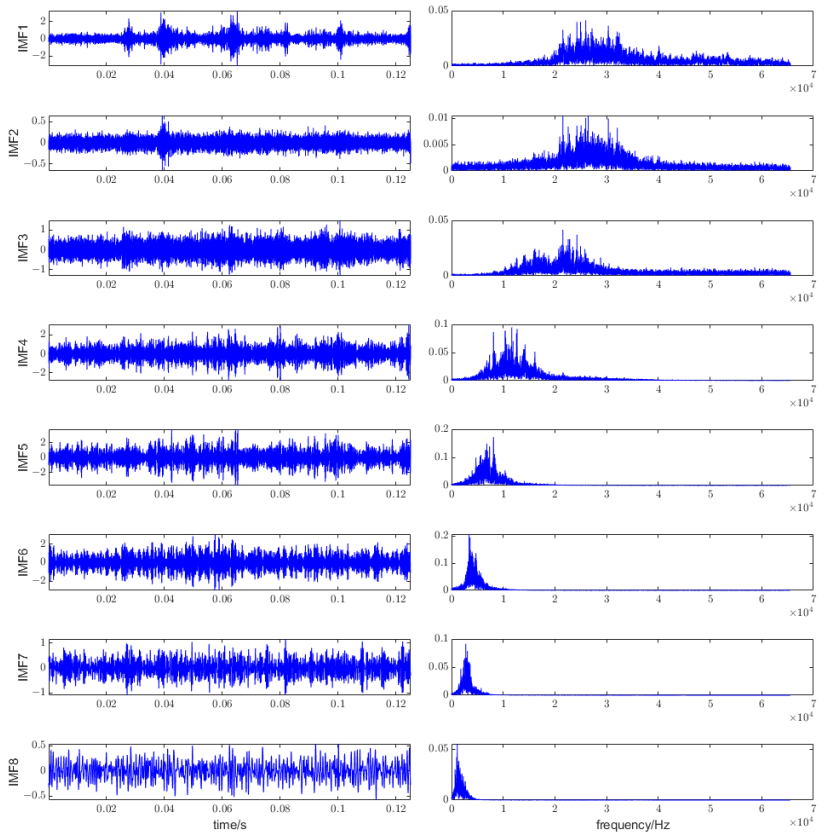

(**a**)

Figure 10. *Cont.*

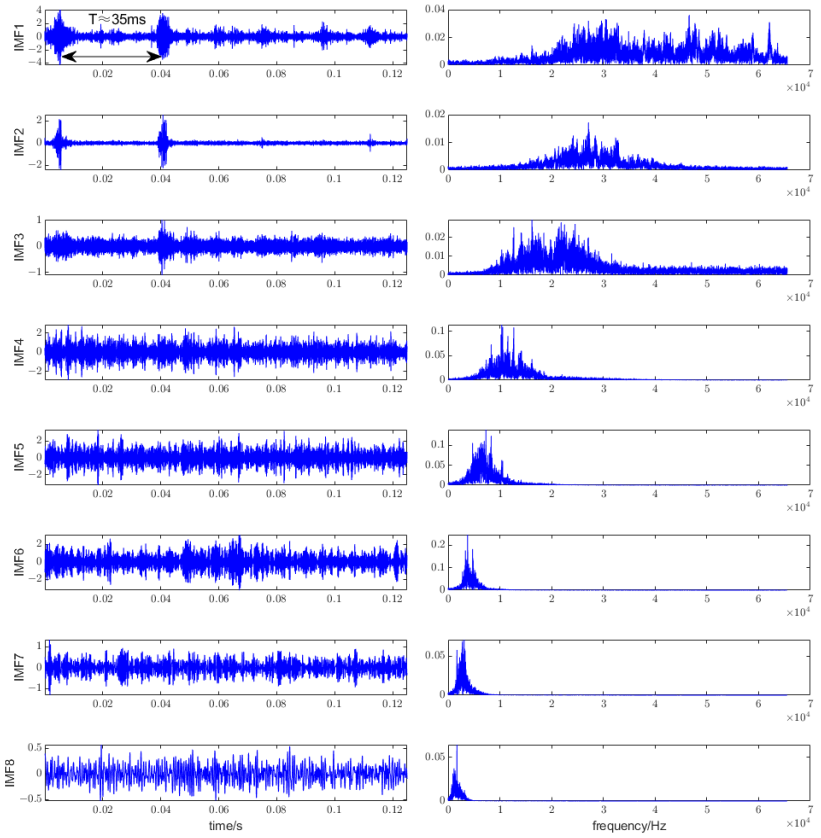

(**b**)

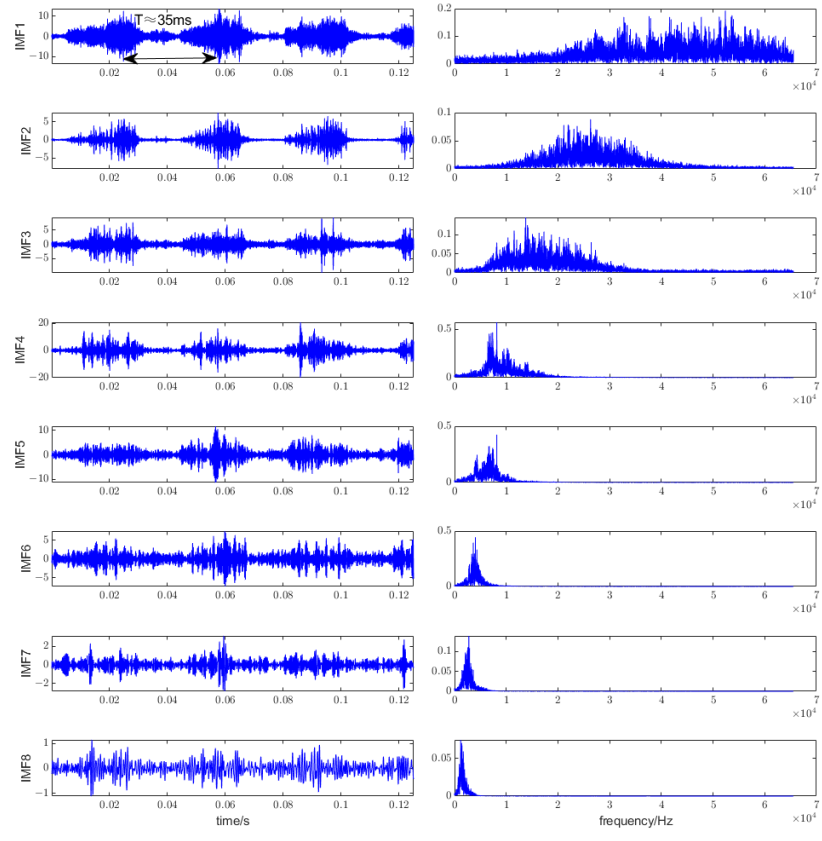

(**c**)

Figure 10. CEEMDAN results: (**a**) no cavitation; (**b**) cavitation inception; (**c**) full cavitation.

In order to compare the effects of different multiscale entropy and decomposition methods on cavitation feature extraction, three kinds of adaptive decomposition methods including CEEMDAN, EMD and VMD (variational mode decomposition) and three kinds of multiscale entropy values including RCMFDE, RCMDE (refined composite multiscale dispersion entropy) and MFDE (multiscale dispersion entropy) are adopted to calculate results of CEEMDAN-RCMFDE, CEEMDAN-RCMDE, CEEMDAN-MFDE, EMD-RCMFDE and VMD-RCMFDE, which are shown in Figure 11. Due to space limitation, only the computation results of IMF1 are listed for analysis. It can be observed from Figure 11a that the entropy values of the measured noise in the three tests conditions are mixed together and not easy to recognize when the scale is small. As the scale increases, the entropy values in different test conditions become easy to recognize, which illustrates the need for multiscale analysis. According to the comparison of Figure 11a–c, the dispersion degree of the entropy values of the three test conditions in Figure 11b,c is smaller than that in Figure 11a, indicating that CEEMDAN classification method has a notably better effect on extracting cavitation features than EMD and VMD. In Figure 11d,e, it is still more difficult to recognize the result of different tests than in Figure 11a, indicating that the RCMFDE has a certain advantage over RCMDE and MFDE in judging the state of cavitation.

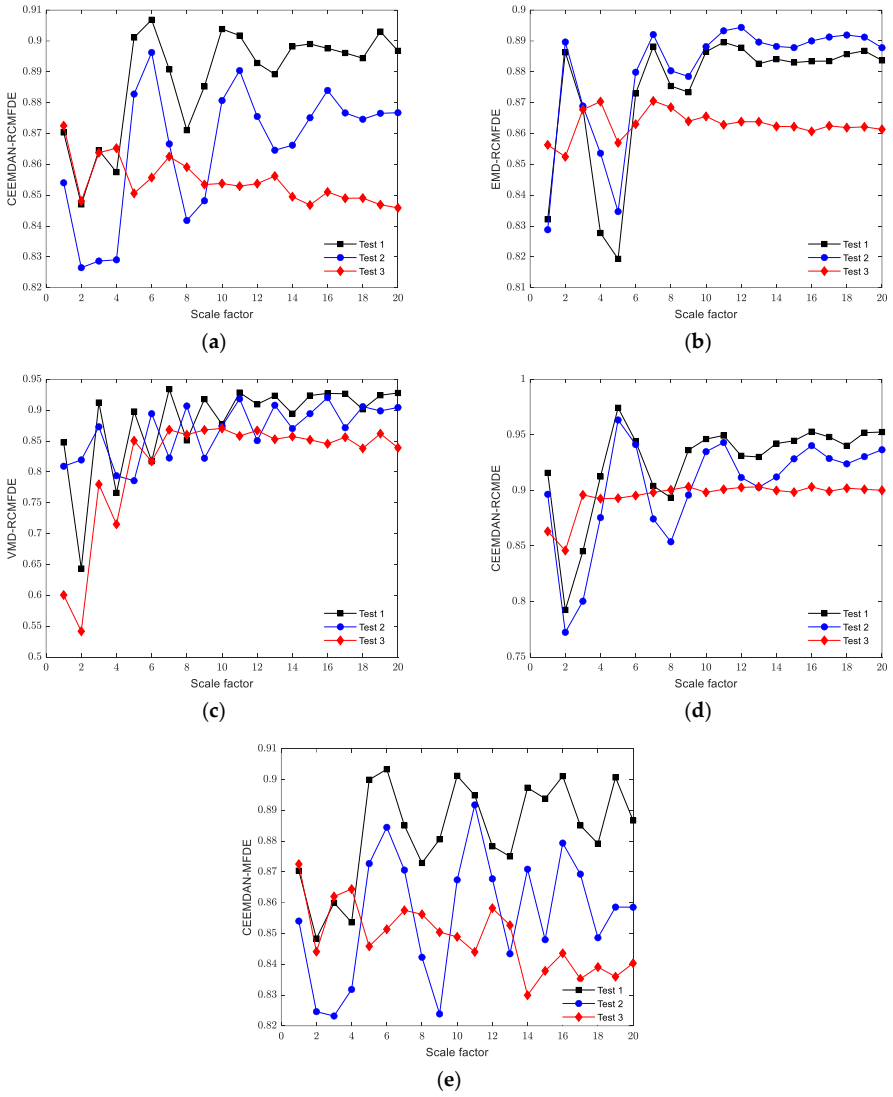

Figure 11. Relation between entropy and scale factor by different features under three test conditions: (**a**) CEEMDAN-RCMFDE; (**b**) EMD-RCMFDE; (**b**) VMD-RCMFDE (**d**) CEEMDAN-RCMDE; (**e**) CEEMDAN-MFDE.

4.2. Diagnosis Results and Analysis

All the raw signals are divided into a total of 720 non-overlapping samples (240 × 3) with a length of 16384, of which 75% are used as training set and 25% as testing set. CEEMDAN is executed for each sample and RCMFDE of the first three IMF components are calculated. Then the hybrid optimization SVM based on Relief-F and PSO is applied to the training set. The PSO initialization parameters are displayed in Table 5.

Table 5. Parameters of PSO-SVM.

G	N	c_1	c_2	w	c	g
100	20	1.5	1.7	1	[0.1, 100]	[0.1, 100]

The identification accuracy with the number of features selected by Relief-F of the training set is shown in Figure 12. It can be seen that the accuracy grows with the number of features when the number is less than 20. Nevertheless, when the number of features is 25 to 45, the accuracy is a little lower than that when the number of features is 20, indicating the negative impact of redundant invalid features on classification. When the number of features is greater than 45, the recognition accuracy is improved restrictedly compared to that when the number of features is 20. Considering the identification accuracy and computational efficiency, the number of features in this paper is set to 20. The PSO optimization process of SVM parameters is shown in Figure 13. It can be seen that with the increase in iterations, the accuracy keeps improving and eventually reaches 90.93%; the optimized penalty factor c is 53.05, and the kernel parameter is 0.82.

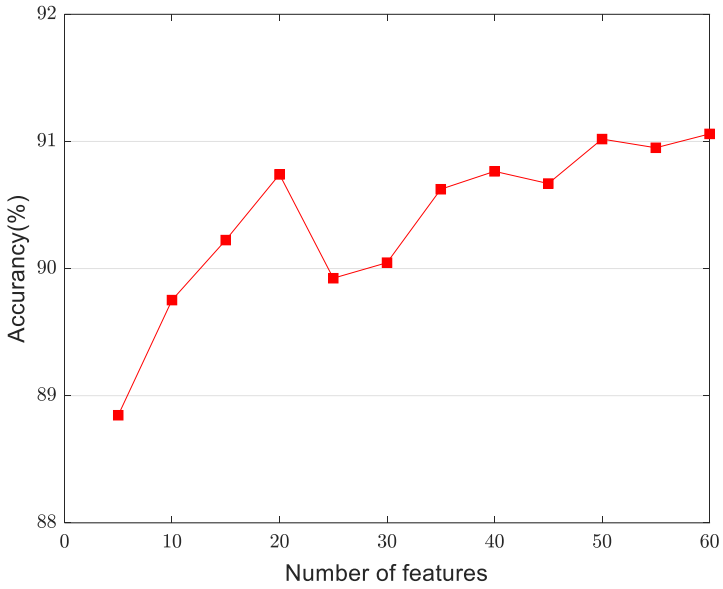

Figure 12. Identification accuracy with number of features selected by Relief-F.

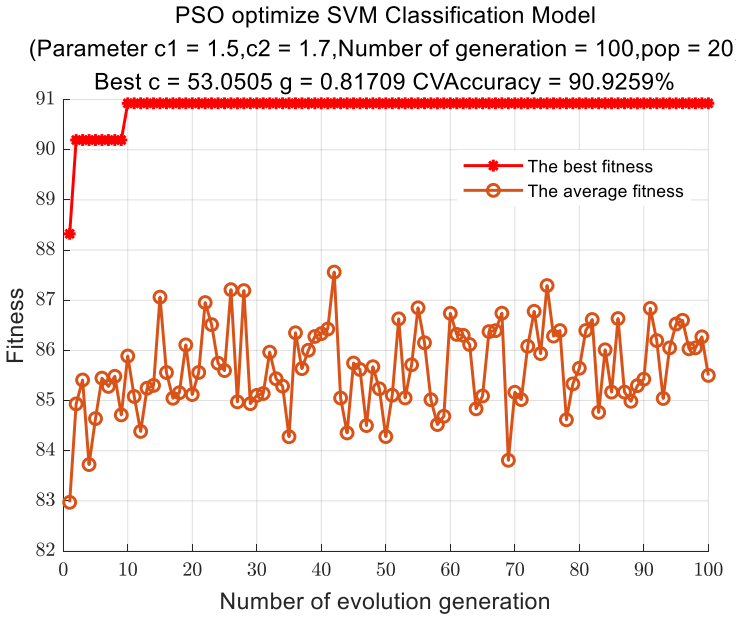

Figure 13. PSO optimization process of SVM parameters.

The identification result of the test set is shown in Figure 14. The results show that the recognition accuracy of severe cavitation samples can reach 100%, while the recognition rate of non-cavitation samples and slight cavitation samples is slightly lower, which are 86.7% (52/60) and 86.7% (52/60), respectively. The overall accuracy of the test set is 91.1% (164/180).

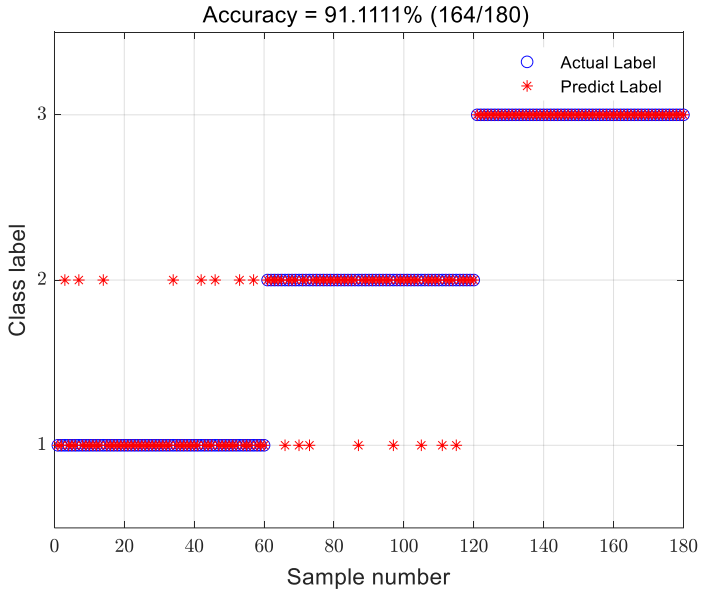

Figure 14. Identification results of the testing set.

4.3. Comparison with Other Methods

In order to demonstrate the superiority of the hybrid optimization SVM proposed in this paper, two other common filter-based feature selection methods, including the Fisher-ratio [33] and Laplace score (LS) [34] methods are selected for comparison. The first 5 to 20 features are screened to form feature vectors, and PSO is used to optimize SVM parameters. The identification results of the test sample are shown in Figure 15. It can be seen that the identification accuracy of the method proposed is superior to the methods based on Fisher and LS.

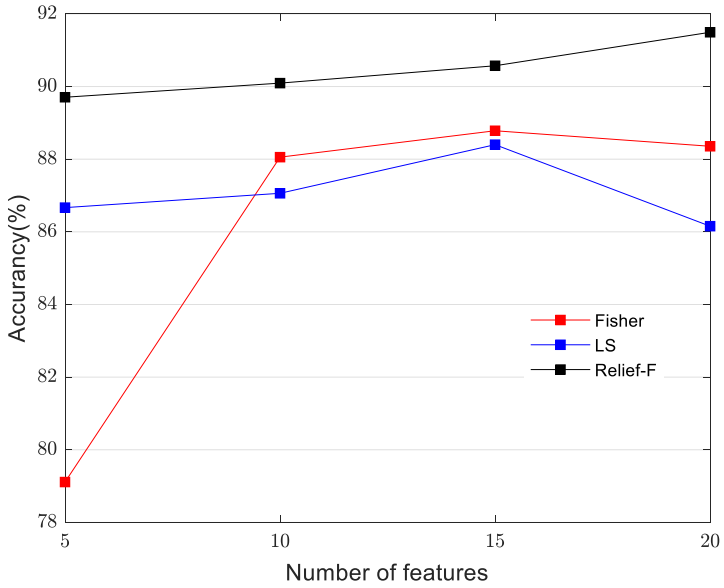

Figure 15. The identification accuracy of different hybrid optimization methods.

To further demonstrate the advancement of the method in this paper, the five characteristics mentioned above, EMD-RCMFDE, VMD-RCMFDE, CEEMDAN-MFDE, CEEMDAN-RCMDE, and CEEMDAN-RCMDE are selected to calculate. Three common machine learning models, back propagation neural networks (BPNN), random forest (RF) and hybrid optimization SVM, are used to classify the samples, respectively. Each method is tested 20 times, and the accuracy of each method is obtained as shown in Figure 16. The result shows that CEEMDAN-RCMFDE is a better feature than other features, and the combination of CEEMDAN-RCMFDE and hybrid optimization SVM can achieve the optimal identification accuracy.

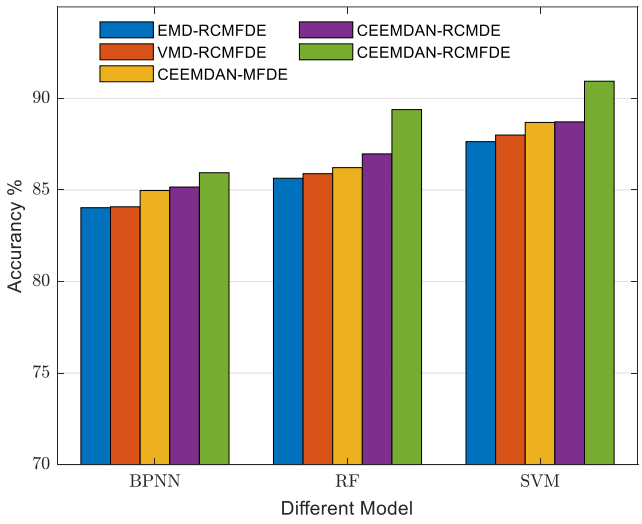

Figure 16. Comparison of identification accuracy of different methods.

5. Conclusions

Considering the nonstationary and nonlinear characteristics of propeller cavitation noise, a novel intelligent identification of propeller cavitation states combining CEEMDAN, RCMFDE, and hybrid optimization SVM is proposed in this paper. First, CEEMDAN is used to adaptively decompose the noise signal to extract useful components related to cavitation. Second, RCMFDE of the first three IMF components are computed as feature vectors. Then, a hybrid optimization SVM classification model is proposed to realize

intelligent identification of propeller cavitation states. The effectiveness of the proposed method is fully verified by the propeller model experiment carried out in the cavitation tunnel. The main conclusions are summarized as follows:

(1) After CEEMDAN preprocessing of the propeller noise signal, cavitation related information exists in the low-order IMF components, and with the deepening of the cavitation degree, cavitation characteristics move up to the higher-order IMF components. CEEMDAN has a finer signal preprocessing effect compared to EMD and VMD.

(2) It is convinced that the nonlinear dynamical entropy theory can be applied to the characterization of propeller cavitation state. Compared with RCMDE and MFDE, RCMFDE applied in this paper has advantages in distinguishing cavitation states.

(3) Relief-F algorithm can optimize the entropy features of high dimensions, and the effect is better than Fisher and LS algorithm. Compared with BPNN and RF, the proposed hybrid optimization SVM model has higher cavitation state identification accuracy.

The method proposed offers a feasible solution for the detection of propeller cavitation. Nonetheless, it should be noted that the noise signal characteristics are weak and unstable at the initial stage of cavitation, which brings great difficulties to the identification of the cavitation state. Future work will focus on improving the characteristics of weak cavitation.

Author Contributions: Conceptualization, Y.L. and L.C.; methodology, Y.L. and L.C.; validation, Y.L. and L.C.; investigation, Y.L.; resources, Y.L.; data curation, Y.L. and L.C.; writing—original draft preparation, Y.L.; writing—review and editing, L.C.; visualization, Y.L.; supervision, L.C.; project administration, L.C.; funding acquisition, L.C. All authors have read and agreed to the published version of the manuscript.

Funding: This research was funded by the Key University and Subjects Development Foundation of Naval University of Engineering under Grant No. 4142Z3391233.

Institutional Review Board Statement: Not applicable.

Informed Consent Statement: Not applicable.

Data Availability Statement: The data presented in this study are available on request from the corresponding author. The data are not publicly available due that the data also forms part of an ongoing study.

Conflicts of Interest: The authors declare no conflict of interest.

Abbreviations

RCMFDE	refined composite multiscale fluctuation-based dispersion entropy
CEEMDAN	complete ensemble empirical mode decomposition with adaptive noise
IMF	intrinsic mode function
SVM	support vector machine
PSO	particle swarm optimization
CIS	cavitation inception speed
STFT	short-time Fourier transform
WVD	Wigner-Ville distribution
TSA	time-domain synchronous averaging
EMD	empirical mode decomposition
FDE	fluctuation-based dispersion entropy
BPNN	back propagation neural networks
RF	random forest
EEMD	ensemble empirical mode decomposition
TVC	tip vortex cavitation
VMD	variational mode decomposition
RCMDE	refined composite multiscale dispersion entropy
MFDE	multiscale dispersion entropy
LS	Laplace score

References

1. Carlton, J.S. Chapter 9—Cavitation. In *Marine Propellers and Propulsion*, 4th ed.; Carlton, J.S., Ed.; Butterworth-Heinemann: Oxford, UK, 2019; pp. 217–260.
2. Kuiper, G.; Jessup, S.D.; Bose, N.; Scherer, O.; Platzer, G.; Perez-Gomez, G. A propeller design method for unsteady conditions. Discussion. Authors' closure. *Trans.-Soc. Nav. Archit. Mar. Eng.* **1993**, *101*, 247–273.
3. Chang, Y.-C.; Hu, C.-N.; Tu, J.-C.; Chow, Y.-C. Experimental investigation and numerical prediction of cavitation incurred on propeller surfaces. *J. Hydrodyn.* **2010**, *22*, 722–727. [CrossRef]
4. Aktas, B.; Atlar, M.; Turkmen, S.; Shi, W.; Sampson, R.; Korkut, E.; Fitzsimmons, P. Propeller cavitation noise investigations of a research vessel using medium size cavitation tunnel tests and full-scale trials. *Ocean Eng.* **2016**, *120*, 122–135. [CrossRef]
5. Chen, L.; Zhang, L.; Peng, X.; Shao, X. Influence of water quality on the tip vortex cavitation inception. *Phys. Fluids* **2019**, *31*, 023303. [CrossRef]
6. Lee, J.-H.; Han, J.-M.; Park, H.-G.; Seo, J.-S. Application of signal processing techniques to the detection of tip vortex cavitation noise in marine propeller. *J. Hydrodyn.* **2013**, *25*, 440–449. [CrossRef]
7. He, Y.; Liu, Y. Experimental research into time–frequency characteristics of cavitation noise using wavelet scalogram. *Appl. Acoust.* **2011**, *72*, 721–731. [CrossRef]
8. Dong, L.; Wu, K.; Zhu, J.-c.; Dai, C.; Zhang, L.-X.; Guo, J.-N. Cavitation detection in centrifugal pump based on interior flow-borne noise using WPD-PCA-RBF. *Shock Vib.* **2019**, *2019*, 8768043. [CrossRef]
9. Widjiati, E.; Djatmiko, E.B.; Wardhana, W.; Wirawan. Analysis of propeller cavitation-induced signal using neural network and wigner-ville distribution. In Proceedings of the IEEE Oceans 2012, Yeosu, Korea, 21–24 May 2012; pp. 1–9.
10. Wu, K.; Xing, Y.; Chu, N.; Wu, P.; Cao, L.; Wu, D. A carrier wave extraction method for cavitation characterization based on time synchronous average and time-frequency analysis. *J. Sound Vib.* **2020**, *489*, 115682. [CrossRef]
11. Azizi, R.; Attaran, B.; Hajnayeb, A.; Ghanbarzadeh, A.; Changizian, M. Improving accuracy of cavitation severity detection in centrifugal pumps using a hybrid feature selection technique. *Measurement* **2017**, *108*, 9–17. [CrossRef]
12. Torres, M.E.; Colominas, M.A.; Schlotthauer, G.; Flandrin, P. A complete ensemble empirical mode decomposition with adaptive noise. In Proceedings of the 2011 IEEE International Conference on Acoustics, Speech and Signal Processing (ICASSP), Prague, Czech Republic, 22–27 May 2011; pp. 4144–4147.
13. Chen, W.; Li, J.; Wang, Q.; Han, K. Fault feature extraction and diagnosis of rolling bearings based on wavelet thresholding denoising with CEEMDAN energy entropy and PSO-LSSVM. *Measurement* **2021**, *172*, 108901. [CrossRef]
14. Yao, L.; Pan, Z. A new method based CEEMDAN for removal of baseline wander and powerline interference in ECG signals. *Optik* **2020**, *223*, 165566. [CrossRef]
15. Gao, B.; Huang, X.; Shi, J.; Tai, Y.; Zhang, J. Hourly forecasting of solar irradiance based on CEEMDAN and multi-strategy CNN-LSTM neural networks. *Renew. Energy* **2020**, *162*, 1665–1683. [CrossRef]
16. Battarra, M.; Mucchi, E. Incipient cavitation detection in external gear pumps by means of vibro-acoustic measurements. *Measurement* **2018**, *129*, 51–61. [CrossRef]
17. Dong, L.; Zhao, Y.; Dai, C. Detection of Inception Cavitation in Centrifugal Pump by Fluid-Borne Noise Diagnostic. *Shock Vib.* **2019**, *2019*, 9641478. [CrossRef]
18. Lee, J.-H.; Seo, J.-S. Application of spectral kurtosis to the detection of tip vortex cavitation noise in marine propeller. *Mech. Syst. Signal Process.* **2013**, *40*, 222–236. [CrossRef]
19. Song, Y.; Liu, J.; Wu, D.; Zhang, L. The MFBD: A novel weak features extraction method for rotating machinery. *J. Braz. Soc. Mech. Sci. Eng.* **2021**, *43*, 547. [CrossRef]
20. Si, L.; Wang, Z.; Liu, X.; Tan, C. A sensing identification method for shearer cutting state based on modified multi-scale fuzzy entropy and support vector machine. *Eng. Appl. Artif. Intell.* **2019**, *78*, 86–101. [CrossRef]
21. Flood, M.W.; Grimm, B. EntropyHub: An open-source toolkit for entropic time series analysis. *PLoS ONE* **2021**, *16*, e0259448. [CrossRef] [PubMed]
22. Li, Y.; Jiao, S.; Geng, B. Refined composite multiscale fluctuation-based dispersion Lempel–Ziv complexity for signal analysis. *ISA Trans.* **2022**, *in press*. [CrossRef]
23. Zhou, F.; Gong, J.; Yang, X.; Han, T.; Yu, Z. A new gear intelligent fault diagnosis method based on refined composite hierarchical fluctuation dispersion entropy and manifold learning. *Measurement* **2021**, *186*, 110136. [CrossRef]
24. Costa, M.; Goldberger, A.L.; Peng, C.-K. Multiscale entropy analysis of complex physiologic time series. *Phys. Rev. Lett.* **2002**, *89*, 068102. [CrossRef] [PubMed]
25. Wu, S.-D.; Wu, C.-W.; Lin, S.-G.; Wang, C.-C.; Lee, K.-Y. Time series analysis using composite multiscale entropy. *Entropy* **2013**, *15*, 1069–1084. [CrossRef]
26. Wu, S.-D.; Wu, C.-W.; Lin, S.-G.; Lee, K.-Y.; Peng, C.-K. Analysis of complex time series using refined composite multiscale entropy. *Phys. Lett. A* **2014**, *378*, 1369–1374. [CrossRef]
27. Ye, M.; Yan, X.; Jia, M. Rolling bearing fault diagnosis based on VMD-MPE and PSO-SVM. *Entropy* **2021**, *23*, 762. [CrossRef] [PubMed]
28. Zheng, J.; Pan, H.; Yang, S.; Cheng, J. Generalized composite multiscale permutation entropy and Laplacian score based rolling bearing fault diagnosis. *Mech. Syst. Signal Process.* **2018**, *99*, 229–243. [CrossRef]
29. Azami, H.; Escudero, J. Amplitude-and fluctuation-based dispersion entropy. *Entropy* **2018**, *20*, 210. [CrossRef] [PubMed]

30. Rostaghi, M.; Azami, H. Dispersion entropy: A measure for time-series analysis. *IEEE Signal Process. Lett.* **2016**, *23*, 610–614. [CrossRef]
31. Kononenko, I. Estimating attributes: Analysis and extensions of RELIEF. In Proceedings of the European Conference on Machine Learning on Machine Learning, Catania, Italy, 6–8 April 1994; Springer: Berlin/Heidelberg, Germany, 1994.
32. Tang, F.; Chen, M.; Wang, Z. New approach to training support vector machine. *J. Syst. Eng. Electron.* **2006**, *17*, 200–219.
33. Zhang, L.; Wu, D.; Han, X.; Zhu, Z. Feature Extraction of Underwater Target Signal Using Mel Frequency Cepstrum Coefficients Based on Acoustic Vector Sensor. *J. Sens.* **2016**, *2016*, 7864213. [CrossRef]
34. He, X.; Deng, C.; Niyogi, P. Laplacian Score for Feature Selection. In Proceedings of the Advances in Neural Information Processing Systems 18, Vancouver, BC, Canada, 5–8 December 2005.